Astrophysics and Space Science (2025) 370:67
https://doi.org/10.1007/s10509-025-04457-0

RESEARCH

Polar caps on the Moon

Jan Kostelecký[1,2] · Jaroslav Klokočník[3] · Aleš Bezděk[3]

Received: 24 March 2025 / Accepted: 23 June 2025

Abstract
The Moon very likely has polar caps, but not as conspicuous as the Earth or Mars; the Moon's caps must be hidden under the surface. The southern polar cap is probably more aquiferous than the northern one. Our indication of ground water at the poles has been obtained by a remote sensing method. We use the gravity aspects, namely the combed strike angles, derived from a global gravity field model of the Moon (now providing the ground resolution ∼10 km already sufficient for this purpose). We cannot estimate the absolute amount of the lunar water, only the contrast between the polar areas and the other regions; the contrast is high, statistically significant – to 8 times more groundwater at the poles. For the southern polar zone, we confirm the results achieved by others, and we do it in a completely independent way. The lunar water is necessary for future permanent human missions on the Moon, like Artemis; they will start near the southern pole. Thus, our findings would have immediate applications. *Observe and download*: https://www.asu.cas.cz/~jklokocn/MOON25_supplements/

Keywords Lunar water · Gravity field model of the Moon · Combed gravity strike angles · Polar ice caps

1 Introduction

The existence of lunar water can be taken, after a long evolution of opinions, as proven (e.g., Crotts 2011, 2012). Water will be necessary for permanent human missions like *Artemis*. The recent landing of *IM-1*/*Odysseus* (Intuitive Machines) at the Malapert A crater (near the south pole) was an important step towards this aim (e.g.: https://www.nasa.gov/feature/artemis/; https://www.intuitivemachines.com/im-1). The polar regions, and especially the southern polar zone, are preferred for their higher chance to keep water (e.g., Cannon et al. 2020). The deeply shadowed craters at the poles, where water could be found in abundance, were identified for Artemis landing (NASA release 22-089). It remains valid, but future astronauts would be happy to find water (and hydroxyl) at any latitude by exploiting specific water-rich areas. Ice could be harvested for drinking and service water, oxygen, and rocket fuel. Some of such potential places have been discovered by analyzing spectrometer data from three independent spacecraft, namely from the Chandrayaan-1 orbiter (Clark et al. 2024); the infrared spectrometer detected water (H_2O) and hydroxyl (OH) out of the poles.

Water in various phases is known not only from the Earth (which is the only celestial body in the Solar System known for sure to have stable bodies of liquid water on its surface), but also on Mars (as ice polar caps and as ground water on other places), e.g., Orosei et al. (2018), and as groundwater on the Moon (more below). It was probably also on Venus (Sohl et al. 2016), can be even on Mercury (Greenwood et al. 2018), under the surface, on Europa, Ganymedes, Callisto (moons of Jupiter), on Enceladus, Titan, Dione, Mimas (moons of Saturn), Triton (moon of Neptun), on Uranus, Neptune, Pluto, Ceres, Vesta, or in comets and asteroids.

We refer here to a broader definition of the polar ice cap as is used in planetary physics, where is no limit to be on surface or beneath, no requirement with respect to size or composition for a body of ice to be termed a polar ice cap, nor any geological requirement for it to be over land. It must only be a body of solid phase matter in the polar region (e.g.,

✉ A. Bezděk
bezdek@asu.cas.cz

J. Kostelecký
kost@fsv.cvut.cz

J. Klokočník
jklokocn@asu.cas.cz

1 Research Institute of Geodesy, Topography and Cartography, CZ 250 66 Zdiby 98, Czech Republic

2 Faculty of Mining and Geology, VSB-TU Ostrava, CZ 708 33 Ostrava, Czech Republic

3 Astronomical Institute, Czech Academy of Sciences, CZ 251 65 Ondřejov, Fričova 298, Czech Republic

Published online: 04 July 2025

Tu et al. 2014). Fanale and Salvail (1989) speak explicitly about "subsurface ice" (they studied Ceres).

Our method, using the gravity aspects (descriptors), Sect. 2 and Supplement SM1, depends on a "sufficient knowledge" of the gravity field meantime already achieved for the celestial body in question. For this purpose, a long series of specific observations of artificial satellites orbiting the bodies (and other data if possible) are needed. One orbiter is not enough (various orbital characteristics are needed, different kinds of observations are welcome). The input to our analyses is always and solely in the form of the Stokes parameters (harmonic potential coefficients) C_{lm}, S_{lm} in the spherical harmonic expansion of the static gravitational potential to selected maximum *d*egree $l = L_{max}$ and *o*rder m (d/o). This is the result of a big inversion from the observational data and quality and resolution of the data dictates reasonable limit of L_{max} (found experimentally). These coefficients depend on the mass density distribution (density variations) inside the body. Their set published to some L_{max} is called gravity (static, global, gravitational) field model (shortly: gravity model). That maximum d/o dictates theoretical global estimate of the ground resolution (GR); definition is in SM1, p. 14.

The "sufficient knowledge" is about the ground resolution, precision and objectivity of their gravity field description depends on the gravity field models available. In the present time, for the Earth with $L_{max} = 2190$, GR is 8-9 km, for $L_{max} = 600$ in the case of the Moon GR $\sim$ 10 km, but for Mars and $L_{max} = 80$, the GR is only 130 km (more in Sect. 2 about Data). Venus and Mercury have to wait for better data. Thus, here we work with the Earth, the Moon, and Mars.

There are four possible sources of the lunar water: the Sun (lunar dust interactions with the solar wind), interplanetary matter bombarding lunar surface, possible past volcanoes, and the atmosphere and ionosphere of the Earth. These sources might supply the Moon for a long time by ions of hydrogen and oxygen to combine water (e.g., Cannon et al. 2020).

The fourth possible mechanism of ice deposition on the Moon has recently been described by Kletetschka et al. (2022). Our Moon periodically moves through the magnetic tail of the Earth (when the Moon is full moon) that contains terrestrial ions of hydrogen and oxygen (Earth's atmospheric escape). A density contrast of ions was measured by Kaguya lunar orbiter. Kletetschka et al. (2022) suggested the accumulation of terrestrial water phase filling the pore-spaced regolith, a portion of which is distributed along the polar regions of the Moon.

For the Earth, Mars, and the Moon we collected figures showing the *Comb* factor, telling us how intensively the strike angles are combed (Sect. 2.2 and SM2). Our main results are presented as statistics in Tables 1a, 1b and as figures in Sect. 3. We find that the Moon has polar caps similarly as the Earth and Mars (but they must be hidden and protected under the surface).

Supplementary files SM1 – SM3 with many figures can be downloaded from: https://www.asu.cas.cz/~jklokocn/MOON25_supplements/.

2 Notes on theory, method and data

2.1 Theory and method

We work with gravity aspects (descriptors), functions of disturbing static global gravitational potential. Theory of the *gravity aspects* has been put together from works from Pedersen and Rasmussen (1990), Beiki and Pedersen (2010), and is summarized in our two books (Klokočník et al. 2017a, 2020a). The reader can see theory and follow the formulae for the individual gravity aspects also in SM1; we cannot repeat the Theory in the main text, only its minimum.

The following is the list of the gravity aspects we work with: the *gravity anomaly* (or disturbance) Δg, the *Marussi tensor* ($\mathbf{\Gamma}$) of the second derivatives of the disturbing potential (T_{ij}), with the second radial component T_{zz}, of two of just three *gravity invariants* (I_j), their *specific ratio* (I), the *strike angles* (θ), SM1:A7, and the *virtual deformations* (vd).

We repeat from Klokočník et al. (2014, 2017a, 2020a, 2021) for easier reading of Sect. 3:

(i) The individual gravity aspects are sensitive in various ways to the underground lithological density contrasts, porosity changes and stress field orientation due to causative bodies. They provide, as the whole group, much more complete information about the ground density variations (the location, shape, orientation, tendency toward 2D or 3D shapes, stress tendencies and tensions).

(ii) The strike angles θ can show directions important for a description of the ground structures providing evidence about the anisotropy (they seem to be parallel to the weakness in the strength of the rock, e.g., the direction schistosity and/or presence of micro-faults). More in SM1. In our figures, the strike angle is shown as abscissa and is counted with respect to the local meridian; red colour means its direction to north of east and blue to south from east.

(iii) The virtual deformations vd (presented as dilation in red or compression in blue colour) show how much energy is stored in the rock material. Around the craters, impact driven expansion causes an irreversible deformation that is exemplified in a motion along the faults through the rock, fractures through the minerals, and even lattice deformations that result in so-called planar deformation features.

We have to keep in mind that the gravity data themselves only indicate geologic structures (anticlines, faults,

salt domes, sediments, etc.), any of which may occasionally contain concentrations of "target deposits" (TD) of various kinds, of practical minerals, salt domes, permafrost (on the Earth), regolith (on the Moon), hydrocarbons (on the Earth and Mars), (water)ice, (ground)water, paleolakes, rifts, faults, volcanic structures, or others.

2.2 Statistics

The strike angles θ have normally diverse directions. The combed strike angles are θ aligned linearly (SM1, Fig. A1-1a versus A1-1b) or to a circle (halo). The theory and statistics for the combed θ may have various forms (Klokočník et al. 2019; Kletetschka et al. 2022 or SM1).

To estimate how intensively the strike angles (in the given region) are combed, we introduced (Klokočník et al. 2019, SM1, pp. 9-11) statistical *Comb* factor. It is a relative value in the interval $\langle 0, 1\rangle$, where 0 means that θ are "not combed" (the vectors of θ are oriented in diverse directions) and 1 means θ are "combed" (perfectly aligned, the vectors of θ are laid down into one direction). The value of $Comb \to 1$ indicates a higher probability of the presence of the lunar water in such areas than when $Comb \to 0$.

The alignments among θ can be: (i) linear, θ are combed in one prevailing direction; typical for valleys, trenches, faults, and catenae, (ii) creating a halo around circular features; the impact craters and basins, or (iii) generating "plates" (blocks of huge size) with the same orientation inside one plate but with the different orientation among the plates. It is not so important which direction is it; what is important is their internal unidirectionality.

2.3 Data

2.3.1 Data for the Earth

We use combined gravitational model (based on satellite and terrestrial data) EIGEN 6C4 Förste et al. (2014). It includes gradiometry data (differential microaccelerometry) from the entire ESA's GOCE mission (2009-2013). This model is expanded to maximum d/o = 2190. The formal global precision of EIGEN 6C4, expressed in terms of Δg, is $\sim$10 mGal. The stability of computation of all necessary functions is ensured by our programs and by software from (Bucha and Janák 2013).

The ETOPO 2022 release (MacFerrin et al. 2022) represents a global, detailed surface topography model of the Earth, an improvement of the previous ETOPO 1 (Amante and Eakins 2009). Their precision in heights (WGS 84) is $\pm$10 m (but not everywhere, as we have intensively tested by comparing the models ETOPO 1, 2022 with other topography models on various localities).

2.3.2 Data for Mars

We used the recent gravity model NASA JPL JGMRO_120 F (Konopliv et al. 2020). The extensive "truncation error tests" (Klokočník et al. 2023a) brought us about choosing the conservative limit d/o=80 to work with (this limit, and not d/o=120, has also been recommended by the authors of the model). The global surface topography of Mars is derived from the MOLA altimeter on board of the Mars Global Surveyor. The accuracy should be $\sim$1 m radially and $\sim$100 m horizontally. The total elevation uncertainty should be "at least 3 m" (Lemoine et al. 2001).

2.3.3 Data for the Moon

We tested two global satellite gravity field models of the Moon derived in the GSFC and JPL NASA, developed from the *GRAIL* observations (*G*ravity *R*ecovery *a*nd *I*nterior *L*aboratory). The models in spherical harmonic expansion are available to (d/o)=1200 and 1500, respectively, GRGM1200A (Lemoine et al. 2014) and GL1500E (Konopliv et al. 2014). We decided to use the GRGM1200A; we used it only to d/o = 600 (as recommended by the authors of the model). A review of lunar missions related to landmark solutions for the gravity field of the Moon is for example in *Table 3.1* of Klokočník et al. (2022b). The formal precision of GRGM1200A should be about 10 mGal globally.

The surface topography of the Moon comes from very successful LOLA (Lunar Orbiter Laser Altimeter), on board of the LRO (Lunar Reconnaissance Orbiter). The heights are given relative to a reference radius of 1737.4 km. A nominal precision of the LOLA altimeter heights is $\sim$10 cm globally.

The figures of the gravity aspects and topography are plotted by *surfer* software in Mercator or polar projection and the animations (for SM2) were prepared by Bezděk and Sebera (2013): https://www.asu.cas.cz/~bezdek/vyzkum/rotating_3d_globe/.

3 Results and discussion

Our results are summarized in Figs. 1a-c for the Earth, Figs. 2a-c for Mars, and Figs. 3a-c for the Moon in the main text, in the tables (Table 1a and 1b), and as additional figures in SM2.

The Earth has the largest concentrations of the highest *Comb* in Antarctica (compare the red spots in Fig. 1c to Figs. 1a, b), as must be expected. We know that many regions of the Earth pose high *Comb* values due to various reasons (recalled shortly in Sect. 2.1 and more details in SM1, pp. 12-14), related to regionally lower density or higher porosity and stress field orientation. Our Fig. 2a – as

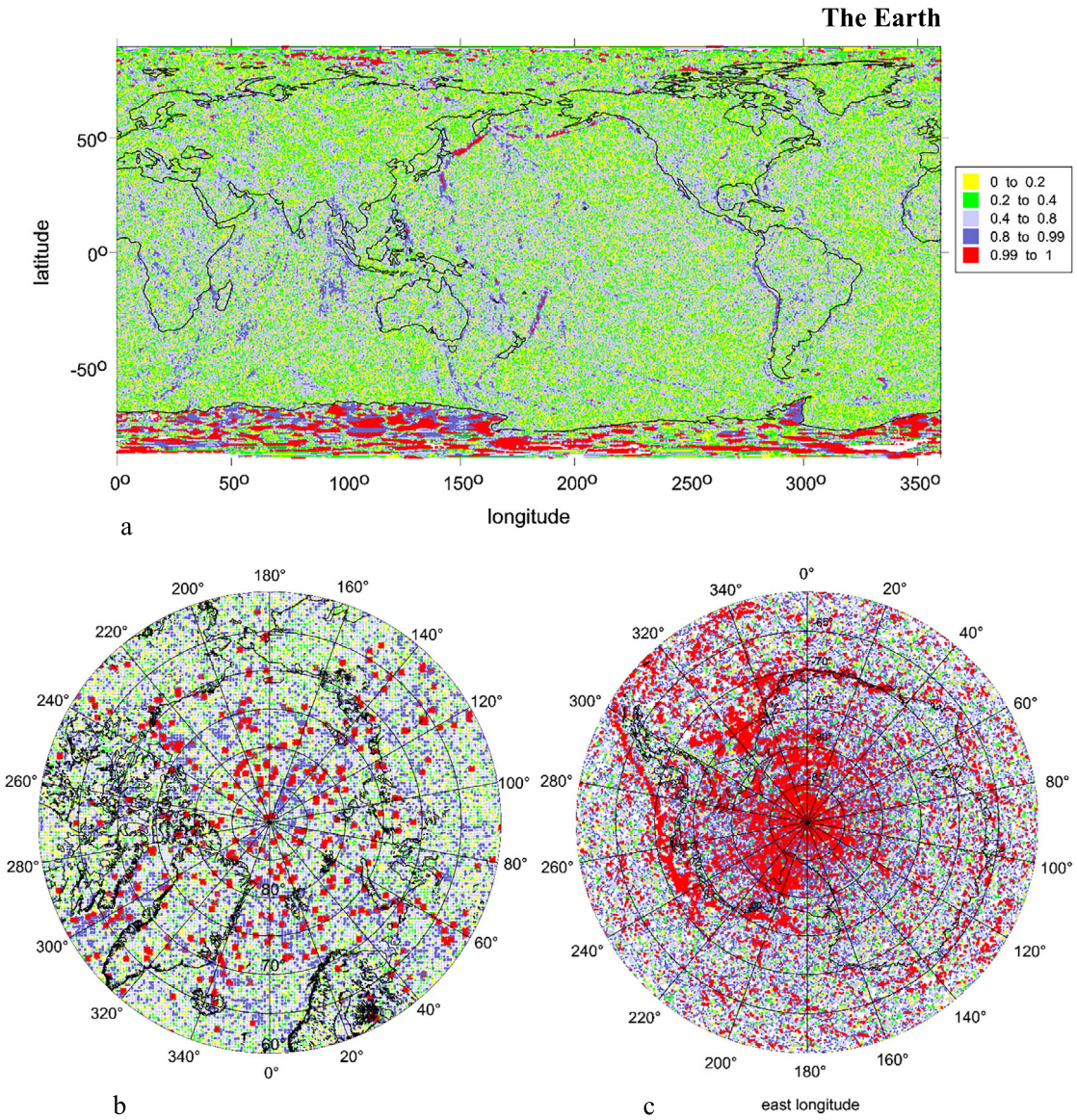

Fig. 1 **a-c**. The *Comb* factors for the Earth (**a** global, **b** north pole zone, **c** south pole zone). The colour scale is the same for all three figures

a general, global view on the Earth – cannot show such details. We refer to other our works with many details (e.g., Klokočník et al. 2014, 2017b, 2020a,b,c, 2022a, 2025a,b).

Mars exhibits the polar caps, the northern is more conspicuous than the southern. It contains H_2O, CO_2 and dust particles. Both caps survive in the local low-pressure atmosphere showing seasonal variations. Again, we receive what was expected – Figs. 2b, c confirms it. The difference between *Comb* at the polar and non-polar regions is relatively small (compare Fig. 2a to 2c). The northern hemisphere had very probably a huge paleo-ocean (SM2:22-29). Now there are lowlands, covered by thick layers of sediments that may contain various ingredients with a lower density or higher porosity material than have the rocks around and on the southern highlands (Klokočník et al. 2023a,b).

On the Moon, the difference between the *Comb* values at the poles and far from them is high (Fig. 3a-c). Tables 1a, 1b show that the difference is statistically significant. Namely the southern polar area shows a large concentration of the highest *Comb* values (Fig. 3c, red spots). It is connected not only with limited illumination at the pole generally but also with an enormous lowland of the Aitken basin. One would expect that highly *Comb* strike angles are only in areas of permanent shadow, may be inside the craters, but they can appear everywhere.

Table 1a shows the ratio $r = P/A$ for all three studied bodies (the Earth, Mars and the Moon). The *Comb* is arbitrary; it was chosen the highest *Comb*>0.99. The "polar" means those regions with the planetographic latitudes $>|70^0|$ and the non-polar is counted for the latitudes

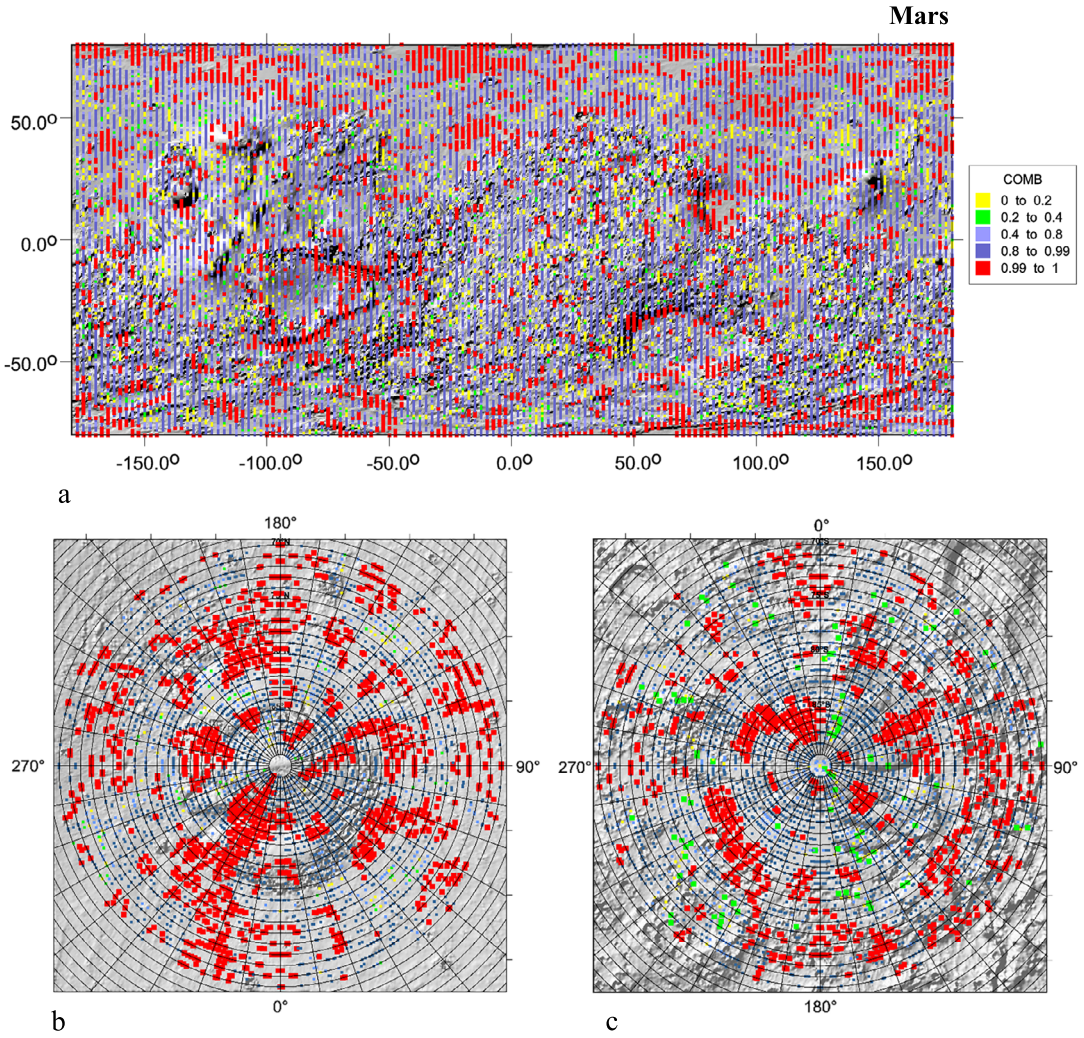

Fig. 2 **a-c**. The *Comb* factors for Mars (**a** global, **b** north pole zone, **c** south pole zone). The MOLA topography. The colour scale is the same for all three figures

(−70,70). The reader can compare r between the polar P and non-polar A areas and among the bodies.

Table 1a clearly demonstrates the known fact that southern polar cap of the Earth is much more conspicuous ($r = 10$) than the northern ($r = 2$). Antarctica is looking like a loaf of Czech bread; the mean thickness of ice is 1.9 km; thickness increases from the seashore to the South Pole up to 4.7 km. The Arctic cannot compete with it. The strike angles react on thick layers of ice first of all, then on the background. Their signal falls quickly, with fourth to eighth power of the distance from the source of density anomaly (see SM1: eqs. A3, A7). Thus, we have received the expected result. The number $r = 10$ is a huge number when we take into account that the planet Earth has water everywhere around the globe; the concentration of water in the "hat" of ice sheet of Antarctica is enormous.

The situation for Mars is more complicated. Table 1a shows a small difference in r between north and south, although we know that the northern cap is bigger and more massive than the southern, looking like a thick pancake sitting on the bottom of the paleo-ocean. The contrast of density between the northern cap and surrounding northern paleo-ocean (with low density/high porosity components) is low (as mentioned above).

Table 1a for the Moon shows partly something expected, partly a surprise. We expect r larger on the south than on the north (8>6). Aitken Basin near the south pole contribute to this result. This area has been chosen for landing of the *IM1*/*Odysseus* and for the pioneer permanent human lunar missions in the frame of the *Artemis* programme (Sect. 1). A ground water is predicted there. The surprise is a high r for both polar regions, $r = 6 - 8$. Compare with the Earth. There is much more groundwater at the poles than in the other localities. Thus, we can speak about the polar caps of the Moon.

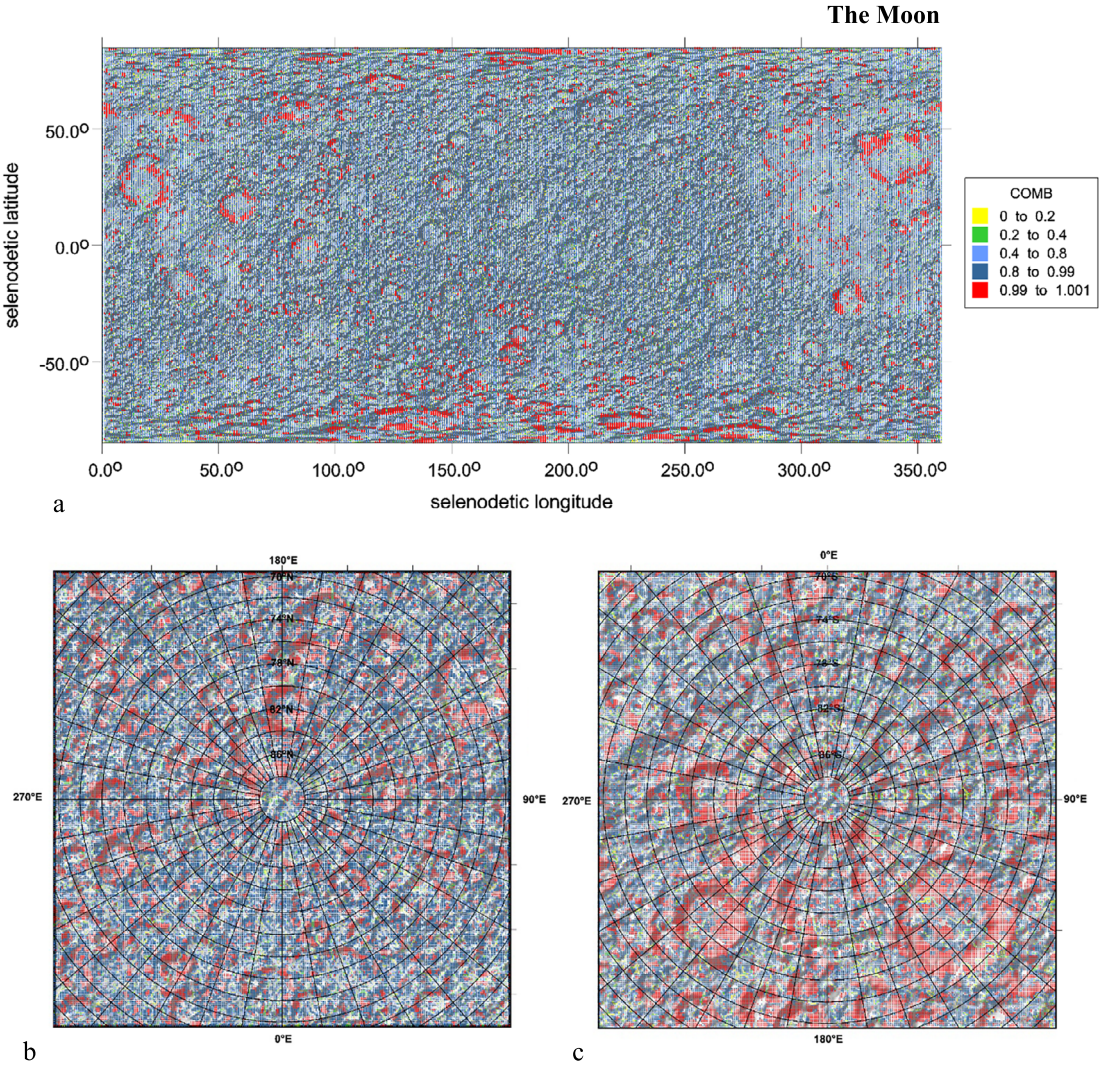

Fig. 3 **a-c**. The *Comb* factors for the Moon and the LOLA topography (**a** global, **b** north pole zone, **c** south pole region). The colour scale is the same for all three figures. All figures have the same colour scale

Table 1a The comparison of the ratios $r = P/A$ for the Earth, the Moon, and Mars for the Comb>0.99 between their polar P and non-polar A areas ["polar" means for planetographic latitudes $> |70^0|$, the non-polar latitudes are within the interval (−70,70)]. The contrast of density between the polar areas (both) on Mars and the non-polar area (−70,70) is low because of the paleo-ocean. It covered mostly the northern hemisphere, but in our statistics in this table we have only one non-polar area and it is extending to both hemispheres (−70,70). Thus, it is useful to add Table 1b with further statistical information

Body		The Earth ♁	The Moon ☾	Mars ♂
polar	south	10	8	1.1
	north	2	6	1.5

Table 1b shows the ratios between Comb>0.99 and Comb<0.99 for the same areas, or P, or A, defined as above, expressed in per cents. This is a complementary information to Table 1a.

Table 1b The ratios "*Comb*>0.99 to *Comb*<0.99" for the same areas, P or A, expressed in per cents

Body		The Earth ♁	The Moon ☾	Mars ♂
polar	south	20%	31%	23%
	north	4%	23%	30%
others		2%	4%	20%

Table 1b for the Earth tells as again how strongly aligned are the strike angles at the southern cap. The Arctic comes out much weaker than Antarctica. For Mars, one can see how high percentage of highly combed strike angles exist in the both caps (23-30%). The Moon at the southern polar area has even 31% of surface with the ratio *Comb*>0.99/*Comb*<0.99, calling again our attention to the hypothetical polar caps of the Moon. We can also

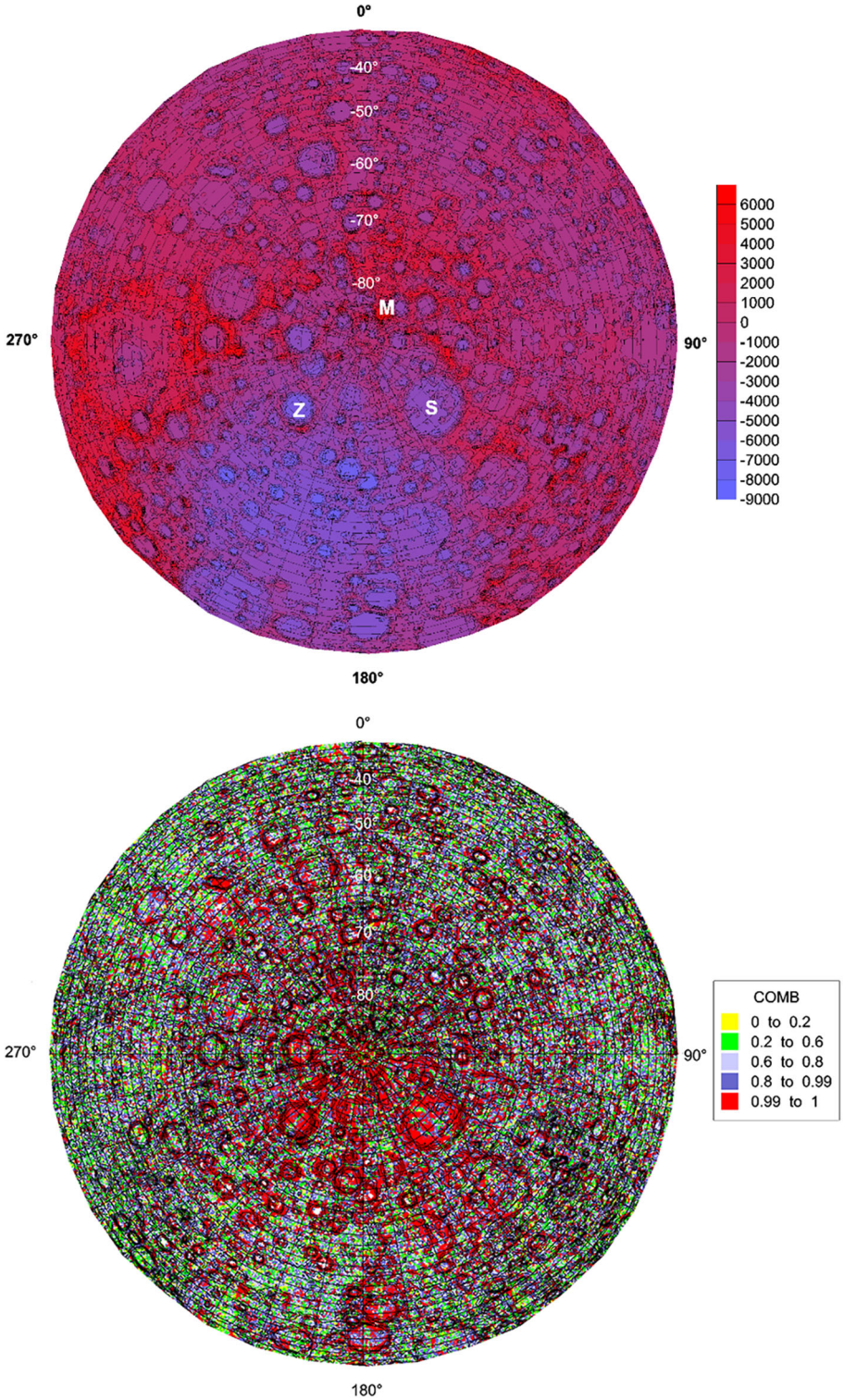

Fig. 4 **a-b**. The *Comb* factors for the Moon together with the LOLA topography [m]: **(a)** the LOLA topography for the whole southern hemisphere; blue circular zone = the Aitken basin, M Malapert, S Schrödinger, Z Zeeman crater **(b)** the topography plus the *Comb* factors. All figures with the *Comb* have the same colour scale

state that the south polar region of the Moon has nearly 1/3 of the surface with statistically higher probability of the lunar water, 8 times more, than the non-polar part of the Moon. There are not the absolute numbers for the amount of water available – we cannot provide them by this method.

There is also well visible difference between two parts of the southern hemisphere: one with the Aitken Basin, the second including all what remains on this hemisphere (Figs. 4a, b). The Aitken Basin is one of the largest impact basins in the Solar System (diameter ~2500 km); it is very deep (to ~8 km). Majority opinion says that the Basin is of impact

origin from time of the heavy bombardment, formed ∼4.2 to 4.3 billion years ago (Pre-Nectarian epoch).

Figure 4b confirms that the Aitken Basin (AB) have more chances for the groundwater than the rest of the southern hemisphere (RSH). We document this difference by means of the statistics with r using *Comb* factor >0.99. Our computation shows that the ratio r AB/RSH of the ratios r AB and r RSH is nearly two.

Let us note about independent results. We have also mentioned the NASA (2022) report about NASA candidate regions (in permanent shadow) for landing Artemis, and Clark et al. (2024). Sanin et al. (2017) and Chuikova et al. (2019) achieved other results for comparison. Measurements of neutron detectors on the board of LRO were conversed to water equivalent hydrogen in the top ∼1 meter layer of the lunar regolith. From the relevant polar maps, hydrogen abundance estimates were inferred; the authors claim that water ice bearing layer may be located below a dry layer of regolith. Their maps and results, concerning the largest craters (their Table 1), fairly agree with our findings (due to the scales of the maps compare their results with Klokočník et al. 2025a).

4 Conclusion

The Moon probably has polar caps (with water ice), like the other terrestrial-type bodies have, but they must be protected against sublimation, and therefore, they survive under the surface. Our remote sensing approach, using the gravity aspects and namely the combed strike angles (Sect. 2.1, SM1), indicates clearly this possibility (see Sect. 3, Tables 1a and 1b, and SM2) in the form of figures (Figs. 1a-c– 4a, b, also figures in SM2) as well as statistically. The strike angles are linearly aligned in the critical places, the *Comb* factor is there approaching 1 (see the red spots in Figs. 3c and 4b). The lunar water is necessary for future permanent human missions on the Moon; they will start near the southern pole. Thus, our findings would have immediate applications.

Acknowledgements We thank for support of the project RVO #67985 815 (Czech Academy of Sciences).

Author contributions Author contributions: Jaroslav Klokočník: Conceptualization, Investigation, Methodology, Writing - original, review and editing, Project administration; Jan Kostelecký: Investigation, Data curation, Software, Visualization; Aleš Bezděk: Data curation, Software, Visualization, Validation, Writing - review and editing, Project administration. All the authors contributed to the data analyses, writing the manuscript, discussion and interpretation.

Funding information Open access publishing supported by the institutions participating in the CzechELib Transformative Agreement.

Data availability The harmonic geopotential coefficients of the gravity field models and topography models are publicly available; figures of the gravity aspects with high resolution (.png files) can be received from Jan Kostelecký on request.

Declarations

The use of AI During the preparation of this work the authors did not use AI technologies.

Competing interests The authors declare no competing interests.

References

Amante, C., Eakins, B.W.: ETOPO1, 1 arc-minute global relief model: procedures, data sources and analysis. NOAA Techn. Memo. NESDIS NGDC **24** (National Geophysical Data Center) (2009). https://doi.org/10.7289/V5C8276M

Beiki, M., Pedersen, L.B.: Eigenvector analysis of gravity gradient tensor to locate geologic bodies. Geophysics **75**, 137–149 (2010). https://doi.org/10.1190/1.3484098

Bezděk, A., Sebera, J.: MATLAB script for 3D visualizing geodata on a rotating globe. Comput. Geosci. **56**, 127–130 (2013). https://doi.org/10.1016/j.cageo.2013.03.007

Bucha, B., Janák, J.: A MATLAB-based graphical user interface program for computing functionals of the geopotential up to ultra-high degrees and orders. Comput. Geosci. **56**, 186–196 (2013). https://doi.org/10.1016/j.cageo.2013.03.012

Cannon, M.K., Deutsch, A.N., Head, J.W., Britt, D.T.: Stratigraphy of ice and ejecta deposits at the lunar poles. Geophys. Res. Lett. **46**, e2020GL088920 (2020). https://doi.org/10.1029/2020GL088

Chuikova, N.A., Rodionova, Z.F., Maksimova, T.G., et al.: Analysis of Lunar terrain altitudes and correlation links between the terrain and gravitational field; preliminary conclusions on the global density inhomogeneities of the Lunar crust. Sol. Syst. Res. **53**, 161–171 (2019). https://doi.org/10.1134/S0038094619020023

Clark, R.N., Pearson, N.C., McCord, T.M., Domingue, D.L., Livo, K.E., Boardman, J.W., Moriarty, D.P., Hendrix, A.R., Kramer, G., Banks, M.E.: The global distribution of water and hydroxyl on the Moon as seen by the Moon Mineralogy Mapper (M^3). Planet. Sci. J. **5**(9), 198 (2024). https://doi.org/10.3847/PSJ/ad5837

Crotts, A.: Water on the Moon, I. Historical overview. Astron. Rev. **6**(8), 4–20 (2011). https://doi.org/10.48550/arXiv.1205.5597

Crotts, A.: Water on the Moon, II. Origins & resources. Astron. Rev. **7**(1), 36–47 (2012). https://doi.org/10.1080/21672857.2012.11519695

Fanale, F.P., Salvail, J.R.: The water regime of asteroid (1) Ceres. Icarus **82**, 97–110 (1989). https://doi.org/10.1016/0019-1035(89)90026-2

Förste, C., Bruinsma, S., Abrykosov, O., Lemoine, J.-M., et al.: The latest combined global gravity field model including GOCE data up to degree and order 2190 of GFZ Potsdam and GRGS Toulouse (EIGEN 6C4). In: 5th GOCE User Workshop, Paris 25–28 Nov (2014)

Greenwood, J.P., Karato, S., Vander Kaaden, K.E., et al.: Water and volatile inventories of Mercury, Venus, the Moon, and Mars. Space Sci. Rev. **214**, 92 (2018). https://doi.org/10.1007/s11214-018-0526-1

Kletetschka, G., Klokočník, J., Hasson, N., Kostelecký, J., Bezděk, A., Karimi, K.: Distribution of water phase near the poles of the Moon from gravity aspects. Sci. Rep. **12**(1), 4501 (2022). https://doi.org/10.1038/s41598-022-08305-x

Klokočník, J., Kalvoda, J., Kostelecký, J., Eppelbaum, L.V., Bezděk, A.: Gravity disturbances, Marussi tensor, invariants and other functions of the geopotential represented by EGM 2008. J. Earth Sci. Res. **2**, 88–101 (2014). ESA Living Planet Symp., 9-13 Sept. 2013, Edinburgh

Klokočník, J., Kostelecký, J., Bezděk, A.: Gravitational Atlas of Antarctica, p. 113. Springer, Berlin (2017a). ISBN 978-3-319-56639-9

Klokočník, J., Kostelecký, J., Cílek, V., Bezděk, A., Pešek, I.: A support for the existence of paleolakes and paleorivers buried under Saharan sand by means of "gravitational signal" from EIGEN 6C4. Arab. J. Geosci. **10**, 199 (2017b). https://doi.org/10.1007/s12517-017-2962-8

Klokočník, J., Kostelecký, J., Bezděk, A.: The putative Saginaw impact structure, Michigan, Lake Huron, in the light of gravity aspects derived from recent EIGEN 6C4 gravity field model. J. Great Lakes Res. **45**, 12–20 (2019). https://doi.org/10.1016/j.jglr.2018.11.013

Klokočník, J., Cílek, V., Kostelecký, J., Bezděk, A.: Gravity aspects from recent Earth gravity model EIGEN 6C4 for geoscience and archaeology in Sahara, Egypt. J. Afr. Earth Sci. **168**, 103867 (2020c). https://doi.org/10.1016/j.jafrearsci.2020.103867

Klokočník, J., Kostelecký, J., Cílek, V., Bezděk, A.: Subglacial and Underground Structures Detected from Recent Gravito-Topography Data (2020a). Cambridge SP. ISBN (10) 1-5275-4948-8; ISBN (13) 978-1-5275-4948-7

Klokočník, J., Kostelecký, J., Varadzinová, L., Bezděk, A., Kletetschka, G.A.: Gravity search for oil and gas and groundwater in Egypt using the strike angles derived from EIGEN 6C4. Appl. Sci. **10**, 8950 (2020b). https://doi.org/10.3390/app10248950

Klokočník, J., Kostelecký, J., Bezděk, A., Kletetschka, G.: Artefacts in gravity field modelling. Acta Geodyn. Geomater. **18**(4), 511–524 (2021). https://doi.org/10.13168/AGG.2021.0036

Klokočník, J., Kostelecký, J., Cílek, V., Bezděk, A., Kletetschka, G.: Atlas of the Gravity and Magnetic Fields of the Moon, p. 263. Springer, Berlin (2022a). ISBN 978-3-031-08867-4. https://doi.org/10.1007/978-3-031-08867-4_2

Klokočník, J., Kostelecký, J., Cílek, V., Kletetschka, G., Bezděk, A.: Gravity aspects from recent gravity field model GRGM1200A of the Moon and analysis of magnetic data. Icarus **384**, 115086 (2022b). https://doi.org/10.1016/j.icarus.2022.115086

Klokočník, J., Kletetschka, G., Kostelecký, J., Bezděk, A.: Gravity aspects for Mars. Icarus **406**, 115729 (2023a). https://doi.org/10.1016/j.icarus.2023.115729

Klokočník, J., Kostelecký, J., Bezděk, A., Cílek, V.: Hydrocarbons on Mars. Int. J. Astrobiol. **22**(6), 696–728 (2023b). https://doi.org/10.1017/S1473550423000216

Klokočník, J., Kostelecký, J., Bezděk, A.: Groundwater at the southern pole of the moon via the gravity strike angles: IM-1 and Artemis. Planet. Space Sci. **256**, 106037 (2025a). https://doi.org/10.1016/j.pss.2025.106037

Klokočník, J., Kostelecký, J., Bezděk, A.: Gravity strike angles to study geological featureson the Earth. Acta Geodyn. Geomater. **22, 2(217)**, 151–182 (2025b). https://doi.org/10.13168/AGG.2025.0011

Konopliv, A.S., Park, R.S., Yuan, D.-N., Asmar, S.W., Watkins, M.M., Williams, J.G., Fahnestock, E., Kruizinga, G., Paik, M., Strekalov, D., Harvey, N., Smith, D.E., Zuber, M.T.: High-resolution lunar gravity fields from the GRAIL primary and extended missions. Geophys. Res. Lett. **41**, 1452–1458 (2014). https://doi.org/10.1002/2013GL059066

Konopliv, A., Park Ryan, S., Rivoldini, A., Baland, R.-M., Le Maistre, S., Van Hoolst, T.: Detection of the Chandler wobble of Mars from orbiting spacecraft. Geophys. Res. Lett. (2020). https://doi.org/10.1029/2020GL090568

Lemoine, F.G., et al.: An improved solution of the gravity field of Mars (GMM-2B) from Mars Global Surveyor. J. Geophys. Res. Planets **106**, 23359–23376 (2001). https://doi.org/10.1029/2000je001426

Lemoine, F.G., Goossens, S., et al.: GRGM900C: a degree 900 lunar gravity model from GRAIL primary and extended mission data. Geophys. Res. Lett. **41**, 3382–3389 (2014). https://doi.org/10.1002/2014GL060027

MacFerrin, M., Love, M., Amante, C.: ETOPO 2022 Release, rev. 1.2, User Guide, NOAA CIRES (2022)

NASA: NASA identifies candidate regions for landing next Americans on Moon, NASA Release 22-089 (2022)

Orosei, R., et al.: Radar evidence of subglacial liquid water on Mars. Science **361**(6401), 490–493 (2018). https://doi.org/10.1126/science.aar7268

Pedersen, B.D., Rasmussen, T.M.: The gradient tensor of potential field anomalies: some implications on data collection and data processing of maps. Geophysics **55**, 1558–1566 (1990)

Sanin, A.B., Mitrofanov, I.G., Litvak, M.L., Bakhtin, B.N., Bodnarik, J.G., Boynton, W.V., Chin, G., Evans, L.G., Harshman, K., Fedosov, F., Golovin, D.V., Kozyrev, A.S., Livengood, T.A., Malakhov, A.V., McClanahan, T.P., Mokrousov, M.I., Starr, R.D., Sagdeev, R.Z., Tret'yakov, A.V., Vostrukhin, A.A.: Hydrogen distribution in the lunar polar regions. Icarus **283**, 20–30 (2017). https://doi.org/10.1016/j.icarus.2016.06.002

Sohl, L.E., Grinspoon, D.H., Aleinov, I., Kelley, M., Clune, T.: Was Venus the first habitable world of our solar system? Geophys. Res. Lett. **43**, 8376–8383 (2016). https://doi.org/10.1002/2016GL069790

Tu, L., Ip, W.-H., Wang, Y.-C.: A sublimation-driven exospheric model of Ceres. Planet. Space Sci. **104**, 157–162 (2014). https://doi.org/10.1016/j.pss.2014.09.002